

B. STYPUŁA*, D. KASPRZYK*, M. HAJOS*

CORROSION BEHAVIOUR OF STAINLESS STEEL IN HOT CONCENTRATED SULFURIC ACID – EFFECT OF FLUORIDE IMPURITIES

KOROZYJNE ZACHOWANIE SIĘ WYSOKOSTOPOWYCH STALI W GORĄCYM STĘŻONYM KWASIE SIARKOWYM – WPŁYW FLUORKOWYCH ZANIECZYSZCZEŃ

The study of corrosion behaviour of stainless steels L904 (0,05C, 1,5Mn, 0,27Si, 0,21Cr, 25,1Ni, 4,4Mo, 1,6Cu) and A211 (0,07C, 2,0Mn, 5,0Si, 18,5Cr, 21Ni, 1,2Mo) were performed in pure concentrated sulfuric acid (96% H₂SO₄, at 90°C) and in the presence of potassium fluoride impurities (5ppm and 10ppm F⁻). The following techniques were used in the study: linear sweep voltammetry (LSV), chronoamperometry, complimented by scanning electron spectroscopy (SEM) and X-ray photoelectron spectroscopy (XPS) analysis. These kinds of steel are extensively used as structural materials in chemical processing and production of sulfuric acid. Corrosion resistance of these steels depend on alloying elements (presence of silicon) and structure of surface layer.

Keywords: stainless steel, corrosion, concentrated sulfuric acid, passivation breakdown, influence of fluoride

Przeprowadzono badania korozyjne stali chromowo – niklowych, L904 (0,05C, 1,5Mn, 0,27Si, 0,21Cr, 25,1Ni, 4,4Mo, 1,6Cu) i A211 (0,07C, 2,0Mn, 5,0Si, 18,5Cr, 21Ni, 1,2Mo) w czystym stężonym kwasie siarkowym (96% H₂SO₄, przy temperaturze 90°C) oraz w kwasie zanieczyszczonym fluorkiem potasu (5ppm i 10ppm F⁻). Stosowano elektrochemiczne techniki polaryzacyjne (woltamperometryczne i chronoamperometryczne) uzupełnione analizą powierzchni przy pomocy metod spektroskopowych, skaningowej spektroskopii elektronowej (SEM) oraz rentgenowskiej spektroskopii fotoelektronów (XPS). Stale te stosowane są jako materiały konstrukcyjne na urządzenia w procesie produkcji kwasu siarkowego. Odporność korozyjna stali zależy od dodatków stopowych (głównie obecności krzemu) i budowy warstwy pasywnej.

1. Introduction

In production lines of sulfuric acid based on roast-gases, the pollution like fluoride ions penetrate the installation as a result of defective work of the wash centre. Until now, very little attention has been paid to the effect of halides ions on the passivation of stainless steels and alloys in the environment. Previous reports [1-2] shows that the presence of chloride ions makes the passivation of stainless steel in concentrated sulfuric acid more difficult. However, the fluoride and iodide ions do not have this influence. Fokin and Gula'ev's [3] proved the inhibiting effect of fluorides on corrosion of austenitic Cr-Ni stainless steel in 67% (14,8M) and 93% (17,3M) sulfuric acid at the temperature of 70°C. No inhibiting effect was seen on pure chromium and ferritic (martensitic) steels with Cr content of 13-28%. The study of the influence of fluoride ions on the anodic

passivation of 316 stainless steel in 64% (10M) sulfuric acid shows that increasing concentration of fluoride ion cause a respective increase in current required for passivation [4]. It has been reported that the effect of F⁻ ions depends on concentration and temperature. At lower temperatures (about 24°C) the lower concentration of fluoride (ok. 1M) seems to protect the metal from corrosion, but at higher concentration or at higher temperature fluoride accelerates attack on the alloy. According to later publication [5, 6], fluorides enhance the local corrosion susceptibility of stainless steels.

Our results indicate the significant effect of composition of stainless steel on its behaviour in concentrated sulfuric acid containing halides impurities [7]. The presented study was conducted to determine the effect of alloying elements on passivation ability of stainless steels: Cr-Ni-Mo-Cu (L904) and Cr-Ni-Si (A211) in hot concentrated sulfuric acid and the influence of fluorides

* AGH – UNIVERSITY OF SCIENCE AND TECHNOLOGY FACULTY OF FOUNDRY ENGINEERING, DEPARTMENT OF CHEMISTRY AND METALS CORROSION, 30-059 KRAKOW, 23 REY-MONTA STR., POLAND

on it. These alloys are usually used to the construction of equipment in the manufacture of concentrated sulfuric acid.

2. Materials and methods

The chemical composition of examined stainless steel are shown in Table 1. The specimens before polarisation were polished using abrasive paper in decreasing order up to 1200 grain size. Subsequently, the samples were washed with distilled water and anhydrite ethanol. The electrochemical measurement were carried out in 96% (17,9M) H₂SO₄ solution containing 10 or 5 ppm of fluorine (as KF), at 90°C. No precaution was taken to eliminate air from the experiments. Polarization was performed using PGZ 301 Voltalab, using the linear sweep voltammetry (at potential scan rate -10 mV/s) and chronoamperometry techniques.

TABLE 1
Chemical composition of studied alloys (in wt. %)

Sample	Concentration [wt.%]									
	Fe	Cr	Ni	Mn	Mo	Cu	Si	C	Co	Ti
A211	55.2	17.74	19.17	0.6	0.33	1.83	4.94	0.01	0.04	0.007
904L	45.97	20.37	24.67	1.6	4.53	1.66	0.57	0.03	0.01	0.23

A platinum wire was used as reference electrode [3]. The measured electrode potential from its platinum-based scale was converted to a standard scale (HNE).

The morphology and chemical composition of the samples surface before and after polarization was examined by scanning electron microscopy (SEM) and X-ray dispersion detector (EDX).

In order to obtain complementary information about chemical compositions of surface films after polarization XPS analysis was carried out.

The XPS spectra were recorded using Al K_{21,2} radiations (1487 eV) from X-ray source operating at 13 kV and 100 mA. Binding energies were referred to the C 1s band from the carbon at 284.8 eV. The relative element content was calculated from the formula (1) according [8].

$$C_k = \frac{I_k/\sigma_k}{\sum_i I_k/\sigma_k}, \quad (1)$$

where: C_k – relative concentration of element k,
 I_k – intensity of line k,
 σ_k – elementary photoionization section.

Composition of layers on the stainless steel were obtained by Ar⁺ ions sputtering the surfaces, using a ion gun mounted in the analysis chamber, under the following conditions: an ion beam voltage 2 kV and a current density of 1 μ A/cm²

3. Results and discussion

It is well known that corrosion behaviour of stainless steels in sulfuric acid depend on their passivation ability. Fig. 1, shows the linear sweep voltammetry curves for the anodic oxidation of both (A211 and L904) alloys in hot (90°C) and concentrated (96% H₂SO₄) sulfuric acid. These curves did not show a sharp current peak, typical for active – passive transition. The dominant characteristic of the both alloys is the wide plateau on the polarization curves (until ~1.0V), with limiting anodic current (about 0.5mA/cm²). Only at higher potential values (at above 1.0V) the distinct anodic current peak appears on polarization curves, in particular for L904 alloy. The peak – separate of primary “pseudo-passive” range from the second one. Similar sharp peak, have been already observed during polarization of austenitic (X1Ni31Cr27Mo3Cu) [9] and duplex (Cr22Ni5Mo3) stainless steel [10]. Until now, the nature of the peak is not quite clear. It may be connected with the oxidation of Fe(II) to Fe(III) and the transformation of sulfates into oxyhydroxides or oxides [9,10] and/or reoxidation of sulfur species (S(0), S(-II), S(IV)), which have been formed during cathodic partial reaction [11]. Furthermore, no transpassivity was observed at the potential below 2 V, and no oxygen was evolved. This finding agrees with those of Tong [12] who studied the anodic behavior of austenitic stainless steels 304 and 316 in 99% H₂SO₄ at the temperature of 30-120°C and found no transpassive region at potential below 4 V.

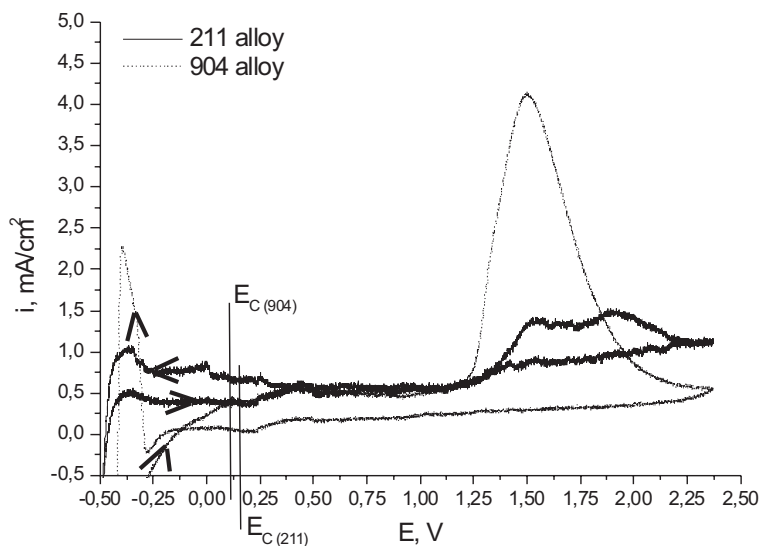


Fig. 1. The linear sweep voltammetry (LSV) curves of examinaion alloys (A211, L904) in 96% H_2SO_4 at 90°C

It is important to pay attention to the difference between the reverse scan of the polarization curves for both alloys. The reverse curve for L904 alloy shows the sharp anodic peak in the active region, which is attributed to the susceptibility to intergranular corrosion [13].

The open-circuit potential (E_c) of A211 alloy as well as L904 are located within the plateau visible before the anodic current peak (in the primary “pseudopassive” range).

The shape of the chronoamperometric curves is shown in Fig. 2. The graph shows that corrosion product remains on the surface and restrains the dissolution of both alloys. The value of anodic current density (between 0.4 and 0.2 mA/cm^2) and their oscillation indicate, the formation of porous passive layer over the surface of both alloys, during anodic polarization.

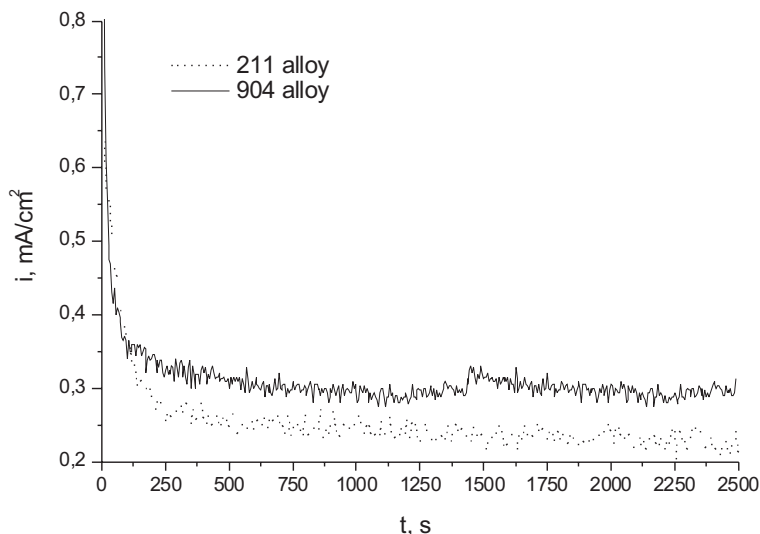


Fig. 2. Evolution of current density versus time of A211 and L904 alloy in 96% H_2SO_4 at 90°C and at $E = 0,6 \text{ V}$

A small contents of fluoride ions ($5\text{ppm} \leq F \leq 10\text{ppm}$) was sufficient to deterioration in the passivation ability of both alloys (A211 and L904) (Fig. 3, 4, 5, 6). They cause the increase of anodic current density in LSV transient, in the whole potential range (Fig. 3, 4). Furthermore, the higher anodic peak is observed on the reverse curves for L904 alloy, in the presence

of fluorides. It is in accordance with some work [5, 6], which found the increase a local corrosion susceptibility of stainless steels and Ni-Cr alloy, in the presence of fluorides. In addition, higher current oscillations appear on the chronoamperometric transient for both alloys (A211 and L904), (Fig. 5, 6).

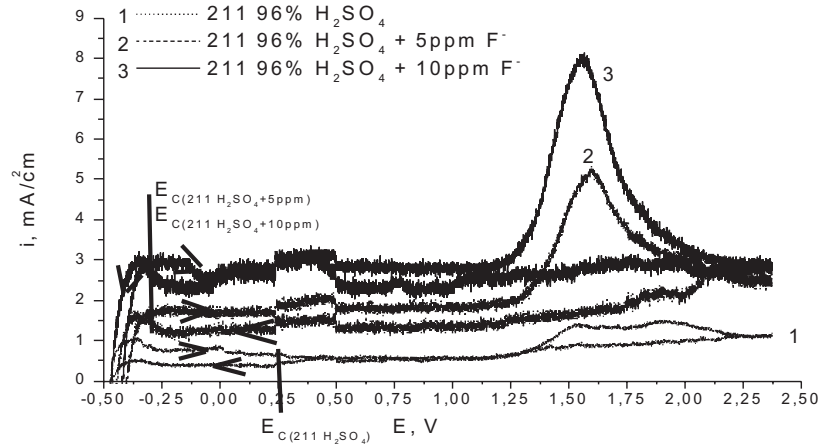


Fig. 3. Influence of fluoride on the linear sweep voltammetry (LSV) curves of A211 alloy in 96% H_2SO_4 at a temperature of 90°C

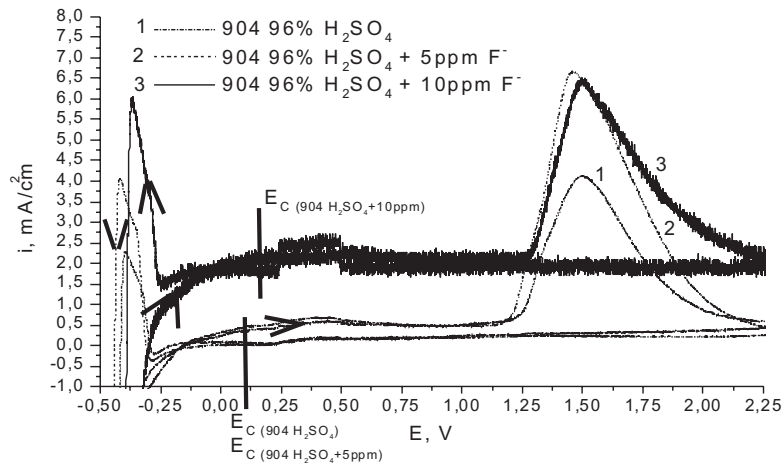


Fig. 4. Influence of fluoride on the linear sweep voltammetry (LSV) curves of L904 alloy in 96% H_2SO_4 at a temperature of 90°C

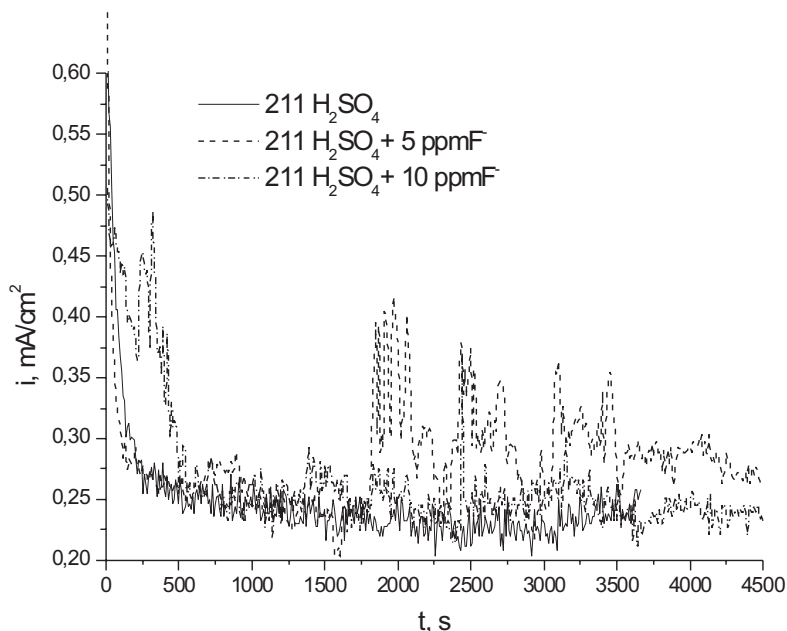


Fig. 5. Influence of fluorid on the chronoamperometric curves of A211 alloy in 96% H_2SO_4 , at 90°C, and at $E = 0,6$ V

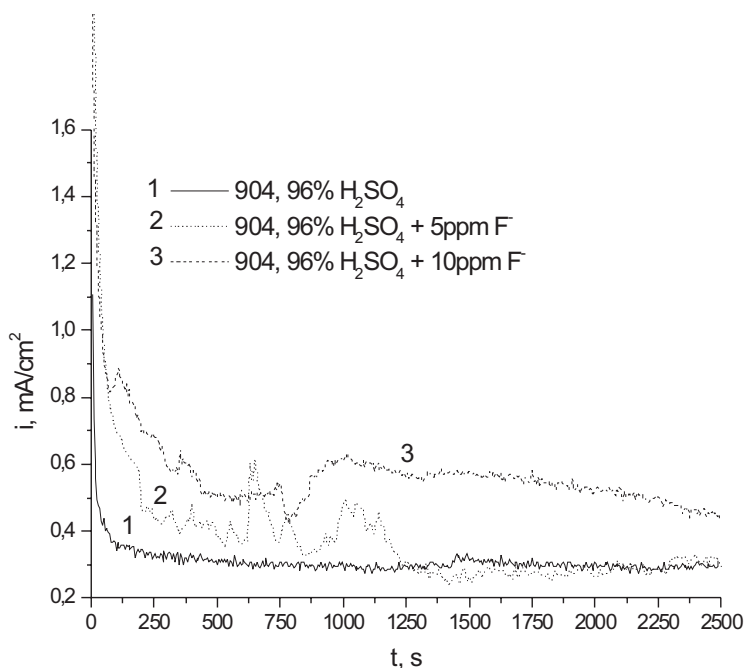


Fig. 6. Influence of fluoride on the chronoamperometric curves of L904 alloy in 96% H_2SO_4 , at 90°C, and at $E = 0,6$ V

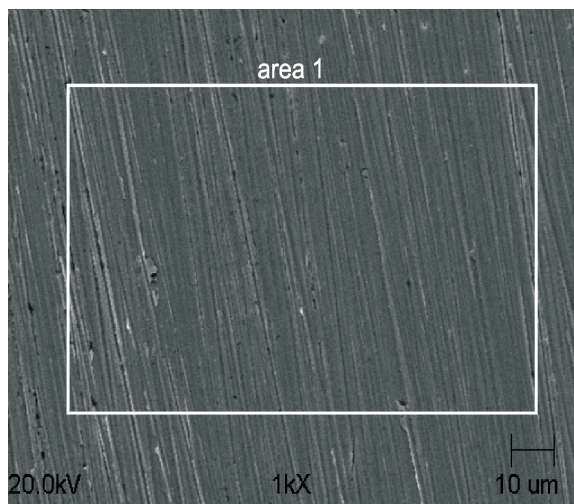
Current oscillation observed during anodic polarization of iron (and a few austenitic stainless steels) in sulfuric acid solutions are extensively studied [14- 20]. According to early suggested [14] a simple periodic current oscillations (at Flade potential) arise as a result of the periodic passivation - activation of Fe electrode occurring due to local pH changes. This basic mechanism was improved by considering the effects of IR – drop and

ferrous salt formation [15]. Recently, it has been shown that small amount of halides induce complex periodic and aperiodic current oscillation for Fe/ H_2SO_4 system [16-18]. The complex oscillation is explained by considering the occurrence of local (pitting) corrosion. The local corrosion may be associated with dissolution of the passive oxide film through the formation of soluble surfaces complexes catalyzed by either H^+ or other

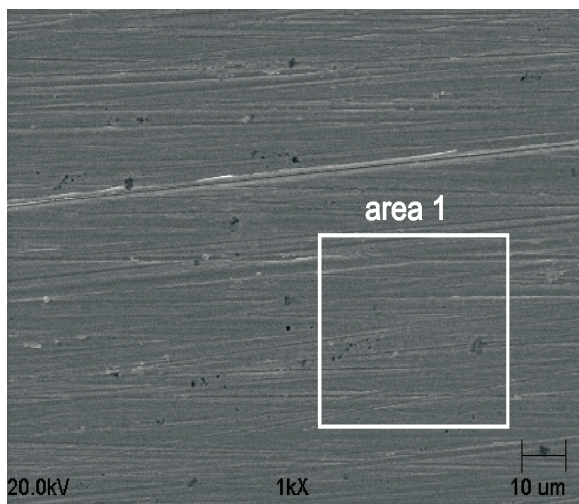
chemical species [19]. Another reason of the oscillations (particularly in pure sulfuric acid) may be arise from the difference in over-potential of cathodic reactions on the oxide or sulfate and on the pure surface of alloys [20]. For that reason, two competitive processes, the formation of a protective film and dissolution, during anodic oscillation, may be proceed according to different mechanism. The current oscillation, in the alloys (A211, L904) / H_2SO_4 system, may be arise from difference in over-potential of cathodic reactions on surface film and on the pure surface. In the presence of fluoride, a local corrosion of the surface film has been additionally occurred, according to local thinning mechanism [21].

3.1. Surface analysis

SEM analysis were performed on both alloys (A211 and L904) after mechanical polishing (rough surface), (Fig. 7a, b) and after exposition (at 0.6 V and 1.9V) in hot pure concentrated sulfuric acid (Fig. 8a, b and 9a, b) The optical visible indicated that the surface of stainless steel containing silicon (A211) was coated with thick layer of corrosion product (Fig. 8a). Whereas, the surface layer on L904 alloy was thin and underwent to local corrosion (Fig. 9a). The preferential attack of grain boundary can be observed at 0.6 V (Fig. 9a) and sub-grains at 1.9 V (Fig. 9b).

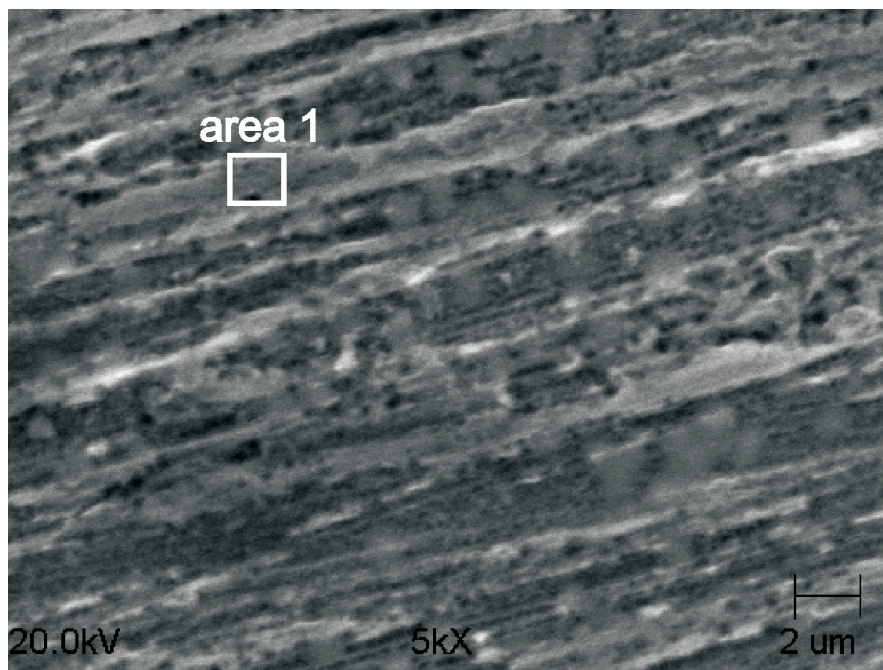


a

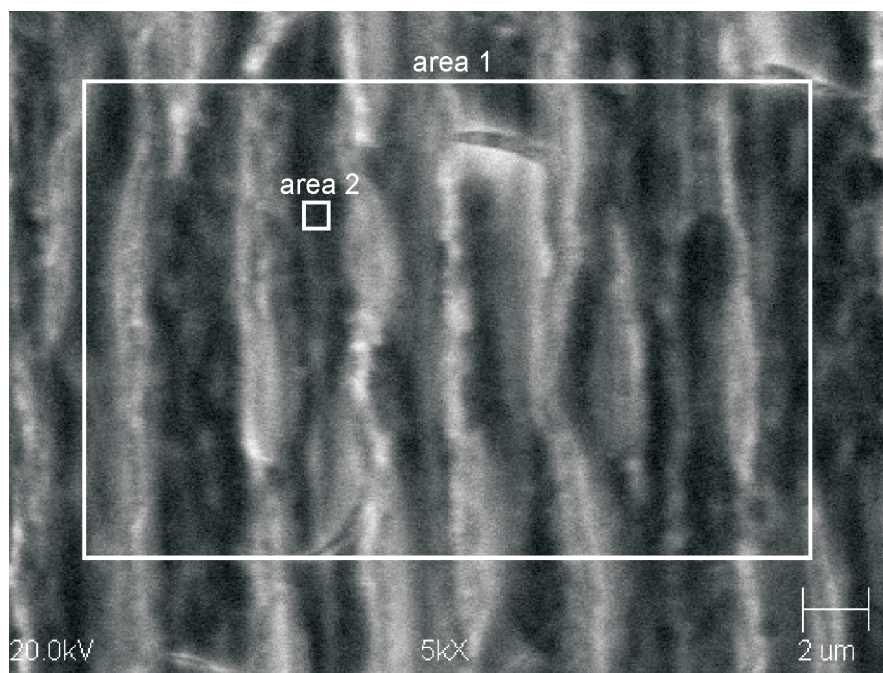


b

Fig. 7. SEM images of rough surfaces of examined alloys (a) A211, (b) L904

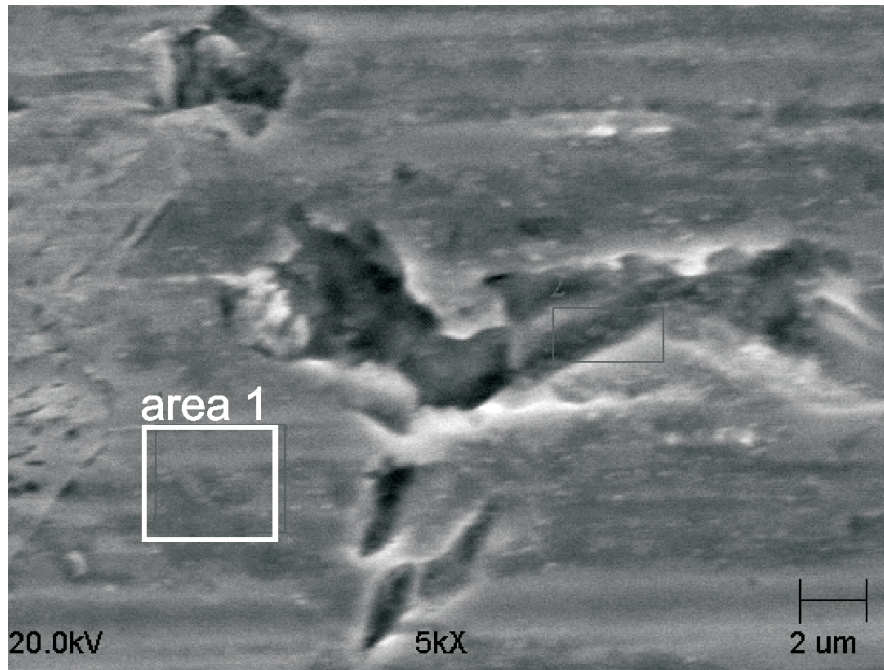


a

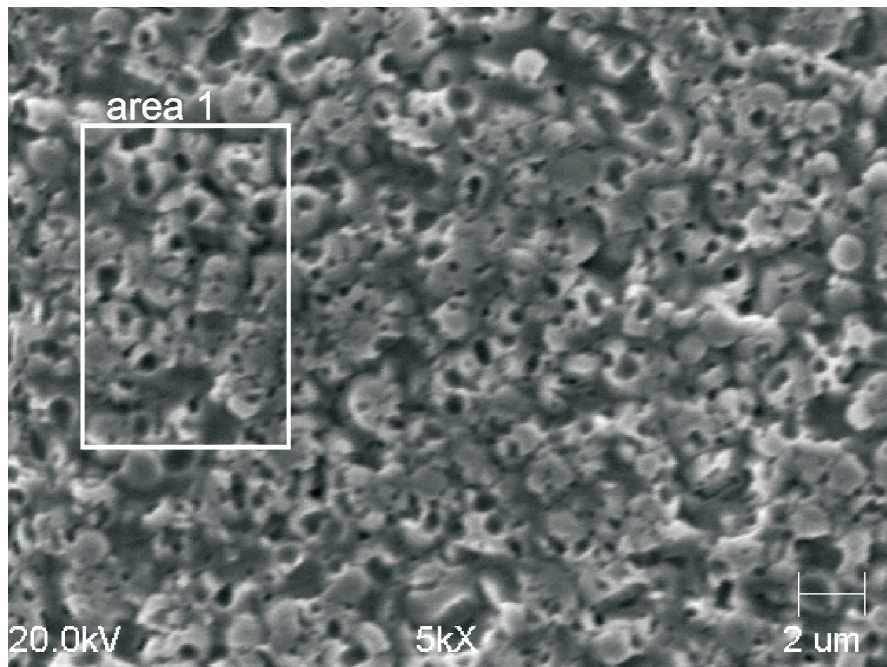


b

Fig. 8. SEM images of A211 alloy after polarization in 96% H_2SO_4 at 90°C (a) $E = 0,6 \text{ V}$; (b) $E = 1,9 \text{ V}$



a



b

Fig. 9. SEM images of L904 alloy after polarization in 96% H_2SO_4 at 90°C (a) $E = 0,6 \text{ V}$; (b) $E = 1,9 \text{ V}$

The chemical composition of surfaces layers determined by SEM/EDX is given in Table 2. The surface layer on A211(Fe-Cr-Ni-Si) alloy, formed in pure sulfuric acid, at $0,6 \text{ V}$, mainly consist of silicon oxide. It follows from high contents of oxygen (about 14 at.%) and small amount of sulfur (about 0.8 at.%) and also

from atomic ratio of elements (Fe:Cr:Ni:Si). The atomic ratio of this elements on the rough surface is about 1: 0.33 :0.30 : 0.19, while the ratio after polarization is 1: 0.30 : 0.31 : 0.27, as shown in Table 2. The comparison of these two indicates the enrichment of the surface in silicon.

TABLE 2

Chemical composition of the sites reported in Fig. 7-9 obtained from SEM/EDX examinations (in at.%)

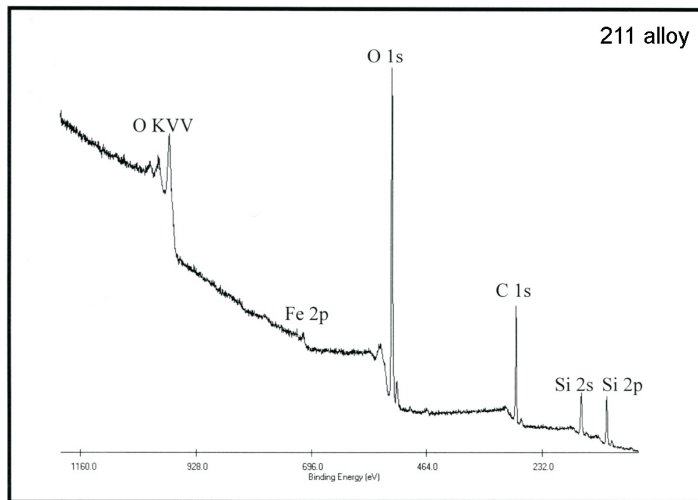
Sample	No of fig./ area	Concentration [at.%]									
		Fe	Cr	Ni	Si	Mn	Mo	Cu	O	S	F
A211	7a/1	54.47	18.43	16.51	10.42	0.16	0	0	0	0	0
A211-H ₂ SO ₄	8a/1	44.88	13.45	14.30	12.26	0.23	0	0	14.04	0.85	0
A211-H ₂ SO ₄ +5ppm F ⁻	9a/1	51.35	16.24	13.43	9.59	0	0	0	4.10	0.50	4.79
A211-H ₂ SO ₄ +10ppm F ⁻	9c/1	43.43	15.07	13.13	10.21	0.27	0	0	7.08	0	10.80
L904	7b/1	44.78	23.02	24.49	1.34	0	0	0	6.37	0	0
L904-H ₂ SO ₄	8c/1	44.19	22.11	19.53	2.37	0	0	0	6.57	5.23	0
L904-H ₂ SO ₄ +5ppm F ⁻	9b/1	35.53	17.09	18.11	2.78	0.43	1.45	2.36	6.51	1.26	14.46
	9b/2	46.26	22.42	19.17	2.58	0.40	1.25	2.93	2.96	0	2.03
L904-H ₂ SO ₄ +10ppmF ⁻	9d/1	43.81	18.86	20.79	0	0	0	0	8.03	3.42	5.09
	9d/2	37.40	15.37	17.08	0	0	0	0	17.08	4.72	8.35
L904-H ₂ SO ₄ 1500mV	8d/1	45.32	21.88	19.47	0	1.48	3.19	1.99	11.72	0	0
A211-H ₂ SO ₄ 1500mV	8b/1	20.53	6.57	4.83	19.25	0	0.34	1.42	47.06	0	0
	8b/2	19.31	6.79	3.91	24.06	0.33	0	0.68	44.91	0	0

The layer on L904 (Fe-Cr-Ni-Mo-Cu) alloy consist of sulfates. This support a relatively small oxygen (6,5at%) and much more sulfur content (about 5at.%) (Tab. 2). Compare with composition of rough surface, the layer is additionally characterized by small impoverished in nickel.

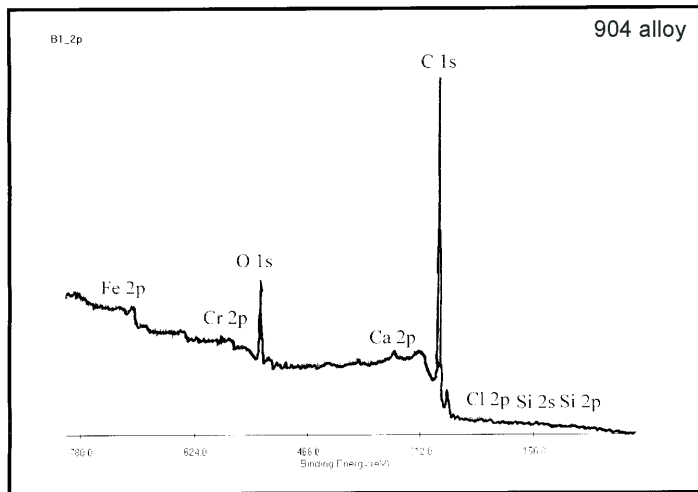
The thickness of the corrosion products on both alloys visibly increases along with the potential above anodic peak, $E \geq 1.9V$ (Fig. 8b, 9b and Tab. 2). The rise of oxygen content and the lack of sulfur are visible. The latter supports the hypothesis that the anodic peak appearing at the potential above 1.0V may be connected with the reoxidation of sulfur species, S(0), S(-II), S(IV), formed at lower potential values as the cathodic component of the process [11].

The XPS measurements (Fig. 10a, b and Tab. 3) as well as SEM/EDX analysis confirmed a high enrichment

in silicon of passive layer formed on A211 alloy. Moreover, they supported that the layer is mainly consisting with silicon dioxide.



a



b

Fig. 10. XPS spectra of alloys surface after polarization $E = 1,9 \text{ V}$ in $96\% \text{ H}_2\text{SO}_4$ at 90°C (a) A211 alloy, (b) L904 alloy

TABLE 3

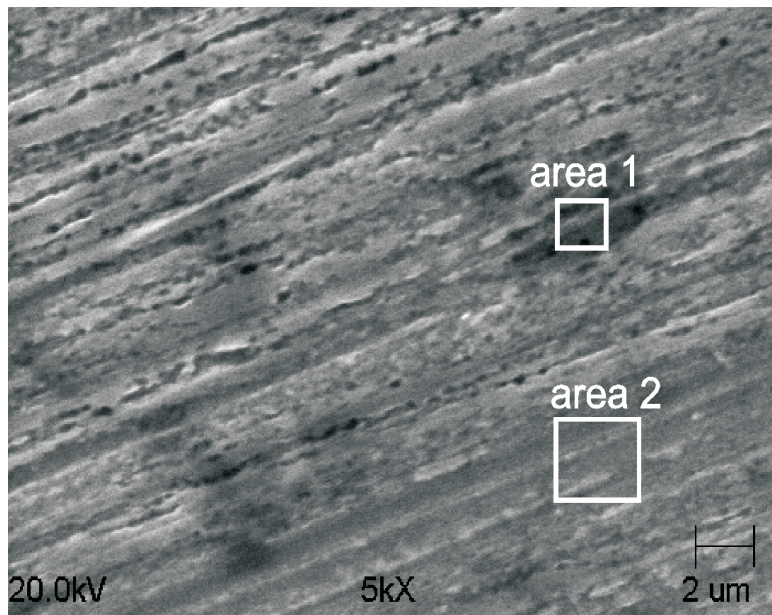
Chemical composition of A211 and L904 alloys surface after polarization at $E = 1,9 \text{ V}$, in $96\% \text{ H}_2\text{SO}_4$, at 90°C from XPS analysis

Element	Concentration					
	Fresh surface, [at.%]		After etching $t=15 \text{ min.}$, [at.%]		After etching $t=30 \text{ min.}$, [at.%]	
	A211	L904	A211	L904	A211	L904
Fe	0,688705	5,084746	2,452316	7,317073	16,96429	24,03846
Cr	0,413223	4,237288	1,362398	4,878049	3,826531	10,09615
Ni	0	1,694915	0,13624	2,439024	1,27551	9,615385
O	67,21763	74,57627	62,80654	75,60976	53,44388	48,55769
Si	31,68044	8,474576	32,97003	8,130081	23,85204	2,403846
Mo	0	5,084746	0,27248	0,813008	0,510204	4,326923
Cu	0	0,847458	0	0,813008	0,127551	0,961538

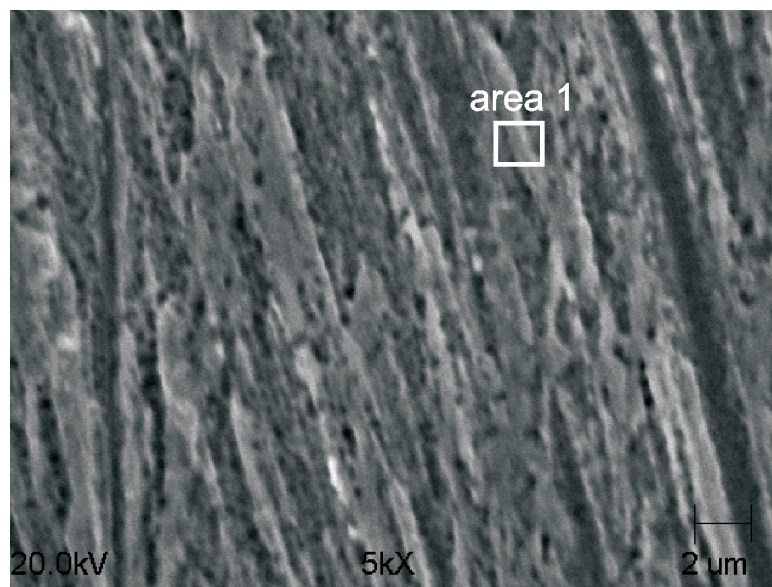
Result of both analyses indicates the change of composition of the layer on L904 (Fe-Cr-Ni- Mo-Cu) alloy, formed above anodic peak (at 1,9V). Similarly to layer on A 211 alloy, no sulfur was found on the surface (at 1.9V). This layer is mainly compound with oxides of iron, chromium, silicon and molybdenum with small amount of nickel and copper (Tab. 3). The formation of oxides

at high potential correlate with higher affinity of metals to oxygen in reaction with sulfuric acid [7]. The affinity fulfils the following row: $Si > Cr > Fe > Mo > Ni > Cu$.

The surface morphology both alloys, after polarization in sulfuric acid containing fluoride ions (5ppm and 10ppm), show figures 11a, b and 12a, b.

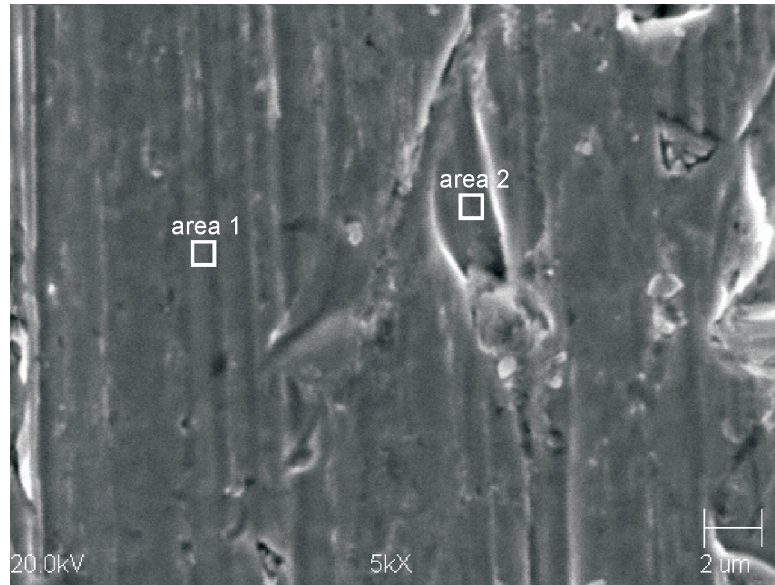


a

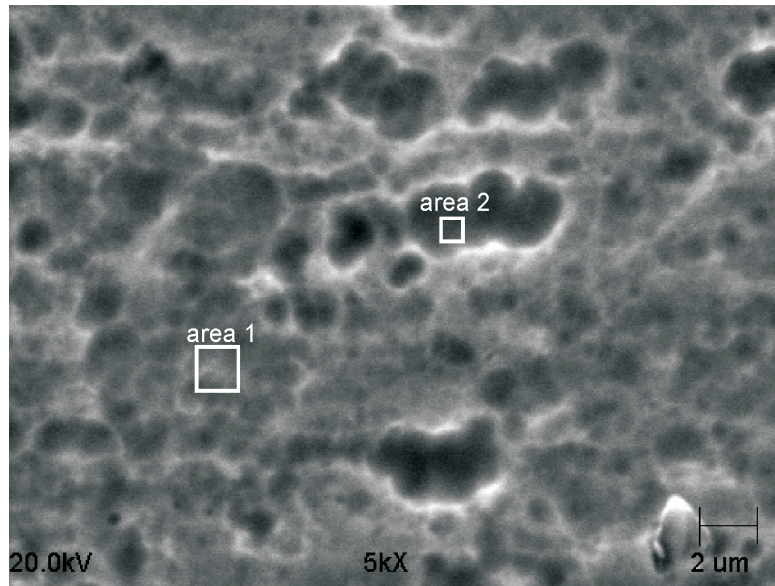


b

Fig. 11. SEM images of A211 alloy after polarization at $E = 0,6 \text{ V}$ in $96\% \text{ H}_2\text{SO}_4$ at 90°C (a)+ 5ppm F^- , (b) + 10ppm F^-



a



b

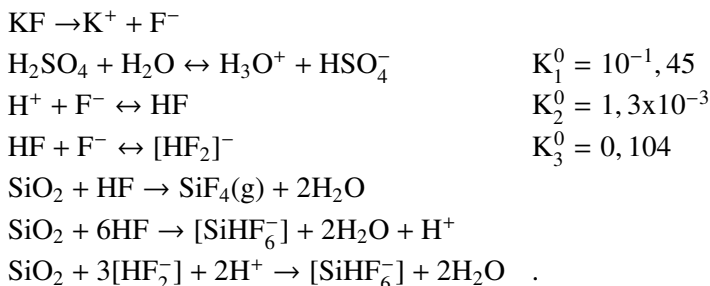
Fig. 12. SEM images of L904 alloy after polarization at $E = 0,6$ V in 96% H_2SO_4 at $90^\circ C$ a) + 5ppm F^- , (b) + 10ppm F^-

The corrosion behavior of these alloys in hot and concentrated sulfuric acid containing fluorides impurities depends on chemical composition of alloys and structure of passive layer.

The addition of fluorides to hot and concentrated sulfuric acid causes strong dissolution of the layer formed on A211 alloy (Fig. 11a, b, Tab. 2). Instead, the local corrosion of L904 alloy, in the presence of fluorides become intensified (Fig. 12a, b). The susceptibility

of alloy L904 to local corrosion was emphasized by a sharp anodic current peak on reverse polarization scan (Fig. 1, 4).

The effect of fluoride ion ($5\text{ppm} \leq F \leq 10\text{ppm}$) on dissolution of A211 alloy is connected with no thermodynamical stability of SiO_2 in the present of fluorides and dissolution with formation of SiF_4 (g) or fluoro-complexes. HF is a weak acid, hence following reactions may occur, in sulfuric acid containing KF:



In accordance with J.S. Judge [22], at the pH below of 1, the concentration of [HF] is higher than [HF₂]⁻ ions, hence dissolution of silicon dioxide mainly occurs according to reaction with HF participation. The chemical dissolution as well as the film formation is favored at irregularity of the surface, such as scratch, crack or edges of oxide islands respectively (Fig. 11a, b, 8a, b).

The presence of small amount fluoride ions (5ppm ≤ F ≤ 10ppm) in the sulfuric acid intensifies local (inter-granular) corrosion of L904 alloy (Fig. 12a, b). The local corrosion in the presence of fluoride ions due to their adsorption on the grain boundaries, as shown SEM/EDX analysis (Fig. 12a, b, Tab. 2). and their catalytic effect on local corrosion, which probably proceeds according to local thinning mechanism [22]. The stronger local corrosion (subgrain corrosion) is observed at the presence of 10 ppm fluorides (Fig. 12b).

4. Summary

The stainless steel containing silicon (A211 alloy) in hot concentrated sulfuric acid (90°C, 96%) coated with a relatively stable layer of corrosion products. The main compound of the layer is silicon dioxide.

Small content of fluoride ions (5ppm ≤ F ≤ 10ppm) in this environment causes a strong dissolution of the surface. It is due to chemical dissolution of SiO₂ with formation of fluoro-complexes.

The L904 alloy (Fe-Cr-Ni-Mo-Cu) in hot and concentrated sulfuric acid (90°C, 96% H₂SO₄) undergoes local (inter-granular) corrosion. The fluoride contamination (5ppm ≤ F ≤ 10ppm) have been adsorbed on grain boundaries and accelerate the local corrosion according to local thinning mechanism.

Acknowledgements

This work was supported by the MEN of Poland (No. 10.10.170.317).

REFERENCES

- [1] S. J. Accellio, N. D. Greene, *Corrosion* **18**, 286, 9(1962).
- [2] J. D. Harston, J. C. Scully, *Corrosion* **25**, 493 (1969).
- [3] M. N. Fokin, V. E. Gula 'ev, *Doklady Akademii Nauk SSSR*, 194, 638 (1970).
- [4] L. Olen, I. R. Riggs, *Corrosion* **19**, 182 (1963).
- [5] I. Sekine et al., *Corrosion Sci.* **36**, 1411 (1994).
- [6] M. A. Rodriguez, *Metallurgical and Materials Transactions* **36**, 1179 (2005).
- [7] B. Stypuła, R. Lebet, P. Grzesiak, *Ochrona przed korozją*, 297 (2002).
- [8] J. H. Scofield, *J. of Spectra and Related Phenomena* **8**, 129 (1976).
- [9] M. Renner, *Material Corrosion* **47**, 246-260 (1996).
- [10] B. Stypuła, J. Banaś, M. Starowicz, *Kwas Siarkowy*, wyd. IOR, Poznań (2003).
- [11] B. Stypuła, M. Starowicz, J. Banaś, *Ochrona przed korozją 11s/A*, 97 (2007).
- [12] H. S. Tong, *Electrochemical Corrosion Testing ASTM 727*, 86-109(1981).
- [13] V. Čihál, *Intergranular Corrosion of Stainless Steels and alloys*, Elsevier, Amsterdam (1984).
- [14] U. F. Franck, R. F. Hugh, *Z. Electrochem* **65**, 156 (1961).
- [15] B. Rush, J. Newman, *J. Electrochem Soc.* **142**, 3770 (1995).
- [16] D. Sazou, M. Pagitsas, C. Georgolios, *Electrochim. Acta* **38**, 2321(1993).
- [17] D. Sazou, C. Georgolios, *Electrochim. Acta* **41**, 147 (1996).
- [18] C. Georgolios, D. Sazou, *J. Solid State Electrochem* **2**, 340 (1998).
- [19] M. Pagitsas et al., *Chemical Physics Letters* **434**, 63 (2007).
- [20] Y. Li, M. B. Ives, K. S. Coley, *Corrosion Sci.* **48**, 1560(2006).
- [21] P. Marcus, V. Maurice, H-H. Strehblow, *Corrosion Sci.* **50**, 2698 – 2704 (2008).
- [22] J. S. Jude, *J. Electrochem. Soc.* **118**, 11, 1772 (1971).